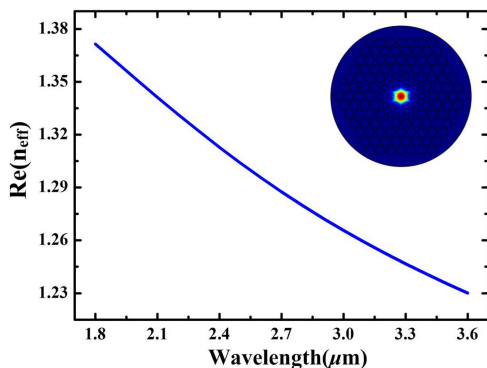


Design of Ultra Large Normal Dispersion ZBLAN Photonic Crystal Fiber and Its Application in Mid-IR Ultra Short Fiber Lasers

Volume 10, Number 6, December 2018

Ying Gao
Jian-feng Li, *Senior Member, IEEE*
Ya-zhou Wang
Yi-Wen Shi
Fei Liu
Kun Li
Jian Yang
Yong Liu, *Senior Member, IEEE*



DOI: 10.1109/JPHOT.2018.2872985
1943-0655 © 2018 IEEE

Design of Ultra Large Normal Dispersion ZBLAN Photonic Crystal Fiber and Its Application in Mid-IR Ultra Short Fiber Lasers

Ying Gao , Jian-feng Li , Senior Member, IEEE, Ya-zhou Wang,
Yi-Wen Shi, Fei Liu, Kun Li, Jian Yang,
and Yong Liu, Senior Member, IEEE

State Key Laboratory of Electronic Thin Films and Integrated Devices, School of
Optoelectronic Information, University of Electronic Science and Technology of China,
Chengdu 610054, China

DOI:10.1109/JPHOT.2018.2872985

1943-0655 © 2018 IEEE. Translations and content mining are permitted for academic research only.
Personal use is also permitted, but republication/redistribution requires IEEE permission.
See http://www.ieee.org/publications_standards/publications/rights/index.html for more information.

Manuscript received August 17, 2018; revised September 20, 2018; accepted September 21, 2018. Date of publication October 1, 2018; date of current version October 29, 2018. This work was supported in part by the National Natural Science Foundation of China under Grant 61722503, Grant 61435003, and Grant 61421002, in part by the Fundamental Research Funds for the Central Universities under Grant ZYWX2016J068, and in part by the International Scientific Cooperation Project of Sichuan Province under Grant 2017HH0046. Corresponding author: Jian-feng Li (e-mail: lijianfeng@uestc.edu.cn).

Abstract: A ZBLAN photonic crystal fiber (PCF) with normal dispersion is theoretically designed and investigated. The designed PCF can provide a large normal dispersion coefficient and a low confinement loss in a broad wavelength range of 1.8–3.6 μm . Especially, the PCF exhibits an ultra large normal dispersion value of -351.3 ps/km/nm and a small confinement loss of 0.05 dB/m at $2.9 \mu\text{m}$. By using the designed PCF as a dispersion compensator in a mode-locked ZBLAN fiber laser, stretched pulse with compressed pulse duration of 1.56 ps is numerically achieved.

Index Terms: Dispersion compensation, mid-infrared fiber laser, photonic crystal fiber (PCF), normal dispersion, ZBLAN fiber.

1. Introduction

Ultra-short pulses with high peak powers operating in the mid-infrared wavelength regime have attracted wide attention considering their significant applications in defense, laser microsurgery, mid-infrared spectroscopy and acting as a pump source for longer wavelength mid-infrared or far-infrared laser generation [1]. For example, ultra-short pulses near $2.9 \mu\text{m}$, targeting a water absorption peak, can be used as an invasive device for laser surgery. Moreover, many strong ro-vibrational absorption lines of some important molecules are located at mid-infrared spectral region. Thus, a mid-infrared super-continuum source pumped by an ultra-short pulse laser can be used to trace molecules. Besides, the ultra-short pulses in this spectral region are also ideal sources to shape and process some special materials, such as plastics, polymer, glasses, etc., and explore efficient physics interaction for high-field physics.

Until now, many efforts have been made in the generation of mid-infrared ultra-short and high peak power pulses. Among them, passively mode-locked fiber lasers are the most promising laser

sources since they are compact, efficient, rugged and not easily influenced by surrounding environment as a result of few bulk components required. We have demonstrated the first ultra-short Ho³⁺/Pr³⁺ co-doped ZBLAN fiber laser at 2.87 μm mode-locked by using semiconductor saturable mirror (SESAM) as a saturable absorber. The pulse width and peak power were 24 ps and ~204 W, respectively [2]. Then, several passively mode-locked ZBLAN fiber lasers utilizing the Fe²⁺:ZnSe crystal [3], SESAM [4], InAs saturable absorber [5], graphene [6], black phosphorus [7], Cd₃As₂-a three-dimensional topological Dirac semimetal material [8] have been demonstrated. As short as 6 ps of pulse duration has been achieved based on saturable absorber [8]. However, no extra dispersion compensators are introduced into the cavity to further shorten the pulses by de-chirping. Thus, a compact, robust, and flexible dispersion method is necessary for the generation of mid-infrared ultra-short pulses.

Generally, there are four kinds of dispersion compensation methods in the mode-locked fiber lasers. Grating pairs, which has excellent performance including high diffraction efficiency, narrow spectral selectivity, and high damage threshold [9], have been extensively used as effective dispersion compensation components in the 1.0 μm [10], 1.5 μm [11], 2.0 μm [12] fiber lasers. Specifically, as short as 28.3 fs pulses with peak power of 24.7 kW have been obtained in an ytterbium-doped mode-locked fiber lasers using a 600 groove/mm grating pairs [8]. However, bulk structure of the grating pairs limits its application in all-fiber structure. Alternatively, chirped fiber Bragg grating (CFBGs) is an attractive method for its all-fiber structure and mature technology, which has been employed in 1.0 μm [13], 1.5 μm [14], 2.0 μm [15] mode-locked fiber lasers. Wherein, 98 fs pulses with 9.8 kW peak power at 1.5 μm have obtained from an erbium-doped mode-locked fiber laser [14]. However, narrow band width of CFBGs limits its application in different wavelength regime and increases the cost. Especially at mid-infrared region, there has no mature technology to inscribe the CFBGs on the ZBLAN fiber. Besides, high NA step-index fiber emerges as an altered dispersion compensation method, which has been widely used in 1.0 μm [16], 1.5 μm [17], 2.0 μm [18] mode-locked fiber lasers. In a ytterbium-doped mode-locked fiber oscillator with 3.6 m long high NA fiber as dispersion compensator, 62 fs pulses with peak power of 116 kW have been achieved [16]. However, long length of this fiber will lead to low repetition rate, high loss and high nonlinearity. Fortunately, by introducing the microstructure in the fiber, a short length fiber can provide large dispersion compensation, which has some merits as high repetition rate and low loss. Moreover, its dispersion can be easily adjusted by changing the geometry parameters. The photonic crystal fiber (PCF) has been widely used in 1.0 μm [19], 2.0 μm [20] mode-locked fiber lasers. Noticeably, by using an anomalous dispersion PCF in an all-fiber-integrated Yb-doped laser [21], pulse duration of 42 fs has been obtained. Considering the high transmission at 3 μm waveband, fluoride fiber is a good candidate for dispersion compensation. In 2015, the first ZBLAN PCF with a high air-filling fraction, a small solid core, nanoscale features and a near-perfect structure was reported [22]. Recently, C. J. Zhao et al [23] have designed a kind of normal dispersion single cladding fluoride fiber by decreasing the core diameter and enlarging its NA, delivering the large chromatic dispersion of -685 ps/km/nm at 3 μm with core size of 1.5 μm and NA of 1.0. However, the designed small core diameter will leads to the large insertion loss.

In this paper, we design a ZBLAN PCF and numerically investigate its dispersion and confinement loss properties. Utilizing the optimized PCF as the dispersion compensator, the pulse evolutions and characteristics in a saturable absorber based mode-locked Er³⁺-doped ZBLAN fiber laser operating at 2.9 μm are studied in detail.

2. Theory

Fig. 1 depicts the transverse cross-section of proposed six rings PCF. The substrate material of the studied PCF is ZBLAN (53ZrF₄-20BaF₂-4LaF₃-3AlF₃-20NaF), whose refractive index can be given by the Sellmeier functions:

$$n^2(\lambda) = 1 + \frac{1.22514\lambda^2}{\lambda^2 - (0.08969)^2} + \frac{1.52898\lambda^2}{\lambda^2 - (21.3825)^2}, \quad (1)$$

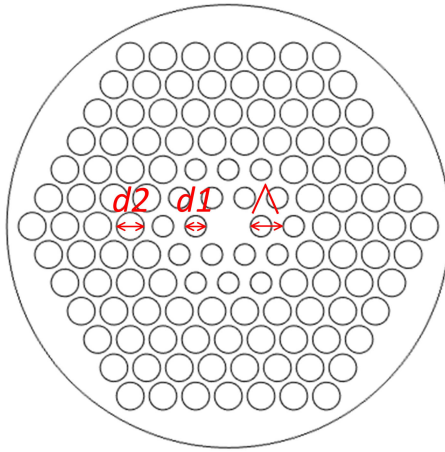


Fig. 1. Cross section of the proposed ZBLAN PCF.

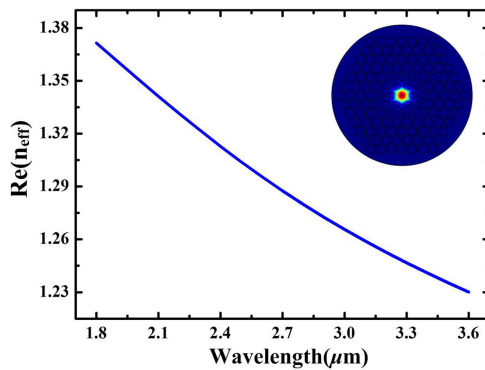


Fig. 2. Effective index of each fundamental mode and its field distribution for ZBLAN PCF for $\Lambda = 1.35 \mu\text{m}$, $d_1 = 1 \mu\text{m}$, $d_2 = 1.3 \mu\text{m}$.

where, λ is the wavelength in μm . The cladding is formed by a triangular lattice of air holes. The air hole pitch is labeled Λ (the distance between the centers of neighboring air holes). The air hole diameter of the two inner rings is labeled d_1 and that of the four outer rings is labeled d_2 , whose refractive index $n = 1$.

Based on the efficient vector finite element method (FEM) with anisotropic perfectly matched layers (PML), the fundamental mode effective refractive n_{eff} as a function of the wavelength is obtained, as shown (the optimal PCF) in Fig. 2. The inset is its corresponding fundamental mode field distribution at the wavelength of $2.9 \mu\text{m}$. The total chromatic dispersion coefficient D , which is used to qualify the amount of chromatic dispersion, can be described as:

$$D = -\frac{\lambda}{c} \frac{d^2 \text{Re}(n_{\text{eff}})}{d\lambda^2}, \quad (2)$$

in ps/km/nm, where λ is the operating wavelength, c is the velocity of light in a vacuum and $\text{Re}(n_{\text{eff}})$ standing for the real part of effective refractive index of the fundamental mode at various wavelength. The confinement loss of the PCF can be obtained by

$$CL = \frac{40\pi}{\ln(10)\lambda} I_m(n_{\text{eff}}) = 8.868k_0 I_m(n_{\text{eff}}), \quad (3)$$

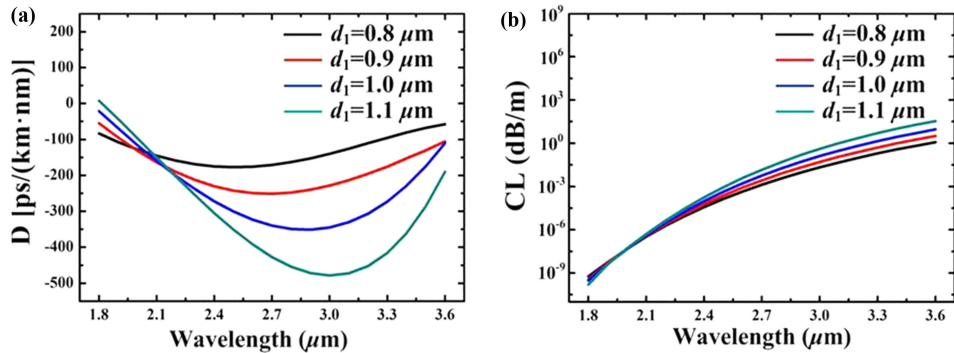


Fig. 3. (a) Dispersion curves and (b) confinement loss for $\Lambda = 1.35 \mu\text{m}$, $d_2 = 1 \mu\text{m}$, and $d_1 = 0.8, 0.9, 1, 1.1 \mu\text{m}$, respectively.

in dB/m, where $Im(n_{\text{eff}})$ is the imaginary part of the complex effective refractive index. The effective mode area A_{eff} is calculated as following:

$$A_{\text{eff}} = \frac{\left(\iint |E(x, y)|^2 dx dy \right)^2}{\iint |E(x, y)|^4 dx dy}, \quad (4)$$

in (μm^2) , where $E(x, y)$ is the fundamental mode electric field of the cross section of the ZBLAN PCF. The nonlinear coefficient of the fluoride PCF is calculated using the following equation:

$$\gamma = \frac{2\pi}{\lambda} \frac{n_2}{A_{\text{eff}}}, \quad (5)$$

where, n_2 is the Kerr coefficient and equal to $5.4 \times 10^{-16} \text{ cm}^2 \text{W}^{-1}$ [24].

With respect to the designed PCF structure shown in Fig. 1, the geometry parameters such as inner d_1 and outer d_2 air hole diameter, air hole pitch Λ have significant influences on the fiber properties, such as chromatic dispersion, nonlinear properties and confinement loss et al. In this section, geometry parameters (d_1 , d_2 and Λ) will be investigated separately to achieve the optimum PCF structural parameters and instruct our and others further design.

3. Results and Discussion

3.1 Simulation Results of PCF

Fig. 3(a) and (b) show the chromatic dispersion and confinement loss as a function of the wavelength with different d_1 , respectively, in which Λ and d_2 are fixed at $1.35 \mu\text{m}$ and $1.3 \mu\text{m}$, respectively. It is observed from Fig. 3(a) that the normal dispersion values increase with increasing d_1 at the range from $2.15 \mu\text{m}$ to $3.6 \mu\text{m}$. The normal dispersion value of the PCF for different d_1 all increase and then decrease with the increasing wavelength. The largest value of -478.3 ps/km/nm is achieved at $3.0 \mu\text{m}$ for $d_1 = 1.1 \mu\text{m}$. Moreover, the peak position of normal dispersion shifts to longer wavelength with increasing d_1 . From Fig. 3(b), the confinement loss of the PCF for different d_1 all increase significantly as the wavelength is increased. Besides, the confinement loss increases with increasing d_1 , especially when the wavelength is beyond $2.5 \mu\text{m}$. It is mainly because smaller d_1 leads to larger effective core diameter, and more guided light will be confined in the core thus decreasing the confinement loss [25]. The confinement losses of 0.009 dB/m , 0.021 dB/m , 0.05 dB/m and 0.15 dB/m at $2.9 \mu\text{m}$ are obtained for d_1 of $0.8 \mu\text{m}$, $0.9 \mu\text{m}$, $1 \mu\text{m}$, and $1.1 \mu\text{m}$, respectively. Thus, the value of normal dispersion, peak position and the confinement loss can be controlled by changing the d_1 .

The influences of d_2 on dispersion curves and confinement losses are also illustrated in Fig. 4. It is observed from Fig. 4(a) that the normal dispersion value increase with decreasing d_2 at the

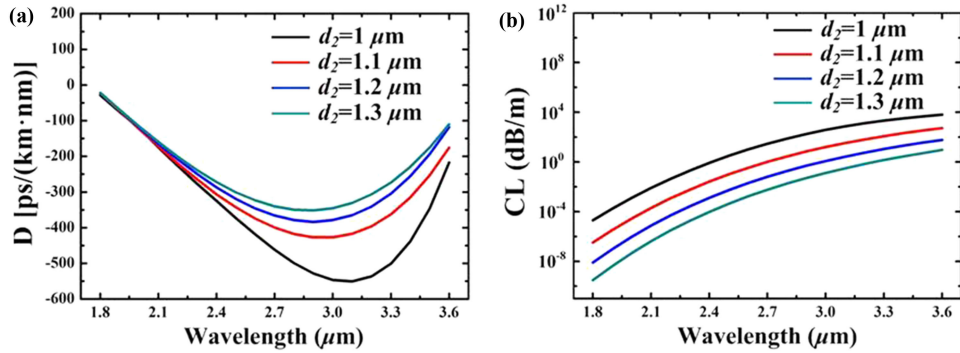


Fig. 4. (a) Dispersion curves and (b) confinement loss for $\Lambda = 1.35 \mu\text{m}$, $d_1 = 1 \mu\text{m}$, and $d_2 = 1.1, 1.2, 1.3 \mu\text{m}$, respectively.

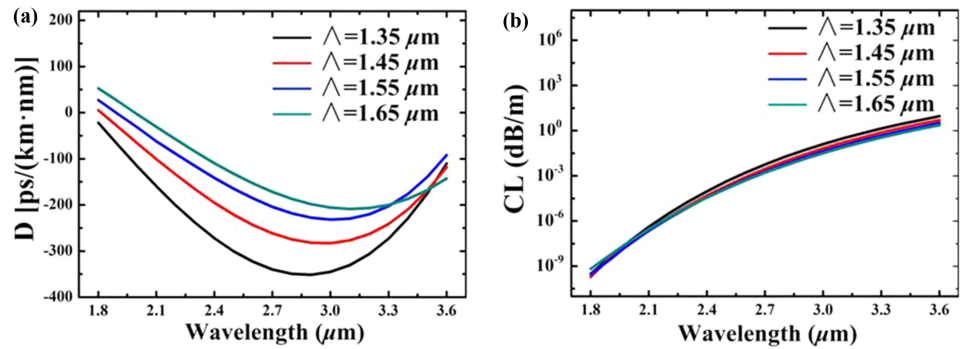


Fig. 5. (a) Dispersion curves and (b) confinement loss for $d_1 = 1 \mu\text{m}$, $d_2 = 1.3 \mu\text{m}$, and $\Lambda = 1.35, 1.45, 1.55 \mu\text{m}$, respectively.

range from $2.2 \mu\text{m}$ to $3.6 \mu\text{m}$. The dispersion values of the PCF for different d_2 all increase and then decrease as the wavelength is increased, and the largest normalized dispersion values D_m of -351.3 ps/km/nm , -383.3 ps/km/nm and -427.5 ps/km/nm and -541.4 ps/km/nm at the corresponding wavelength $\lambda_m = 2.9 \mu\text{m}$, $2.94 \mu\text{m}$, $3 \mu\text{m}$, and $3.07 \mu\text{m}$ are obtained for d_2 of $1.3 \mu\text{m}$, $1.2 \mu\text{m}$, $1.1 \mu\text{m}$ and $1 \mu\text{m}$, respectively. The peak position of normal dispersion shifts to shorter wavelength with increasing d_2 . From Fig. 4(b), the confinement losses increase significantly with increasing wavelength and decrease significantly with increasing d_2 . The confinement losses reach 0.05 dB/m , 0.49 dB/m , 6.96 dB/m and 178.8 dB/m at $2.9 \mu\text{m}$ for d_2 of $1.3 \mu\text{m}$, $1.2 \mu\text{m}$, $1.1 \mu\text{m}$ and $1 \mu\text{m}$, respectively. It is mainly because the effective index of cladding is smaller with larger d_2 , resulting in the larger effective index difference between the core and the cladding. Thus, more light will be reflected and more energy will be confined in the core. The results indicate that increase of d_2 leads to slightly decreased peak dispersion value, but it seriously decreases the confinement loss e.g., when d_2 increases from $1 \mu\text{m}$ to $1.3 \mu\text{m}$, the varied dispersion value is 190 ps/km/nm (almost 54.1 percent) while the confinement loss is decreased by 178.75 dB/m (almost 3735 times) at $2.9 \mu\text{m}$. Accordingly, larger d_2 is more preferred on the condition that it is smaller than the air hole pitch Λ for the structure limits.

Fig. 5(a) and (b) shows the influence of the air hole pitch Λ on the dispersion and confinement loss with the identical d_1 of $1 \mu\text{m}$ and d_2 of $1.3 \mu\text{m}$, and variable Λ of $1.35 \mu\text{m}$, $1.45 \mu\text{m}$ and $1.55 \mu\text{m}$, respectively. From Fig. 5(a) we can see that the normal dispersion value increases significantly with the decreasing Λ at the range from $1.8 \mu\text{m}$ to $3.3 \mu\text{m}$. The dispersion value of the PCF for different Λ all increase and then decrease with the increasing wavelength, the peak values of normal dispersion $D_m = -351.3 \text{ ps/km/nm}$, -283.4 ps/km/nm , -231.9 ps/km/nm , and -208.7 ps/km/nm

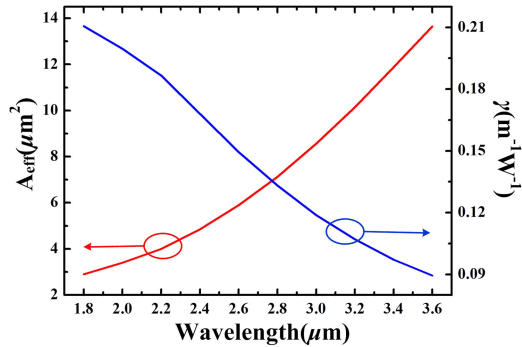


Fig. 6. Effective mode area and nonlinear coefficient for $d_1 = 1 \mu\text{m}$, $d_2 = 1.3 \mu\text{m}$, and $\Lambda = 1.35 \mu\text{m}$.

located at the λ_m of $2.9 \mu\text{m}$, $2.96 \mu\text{m}$, $3 \mu\text{m}$ and $3.1 \mu\text{m}$ are obtained for Λ of $1.35 \mu\text{m}$, $1.45 \mu\text{m}$, $1.55 \mu\text{m}$ and $1.65 \mu\text{m}$, respectively. Thus, the peak position of normal dispersion shifts to longer wavelength with increasing Λ . From Fig. 5(b), the confinement losses of the PCF for different Λ all increase significantly as the wavelength is increased. However, the Λ has negligible effects on the confinement loss. With the increasing Λ , the confinement loss decrease very slightly. The confinement losses are 0.05 dB/m , 0.026 dB/m , 0.017 dB/m and 0.013 dB/m at $2.9 \mu\text{m}$ for Λ of $1.35 \mu\text{m}$, $1.45 \mu\text{m}$, $1.55 \mu\text{m}$ and $1.65 \mu\text{m}$, respectively.

To achieve large normal dispersion and low confinement loss at $2.9 \mu\text{m}$, the optimum parameters of the designed PCF can be chosen as $d_1 = 1 \mu\text{m}$, $d_2 = 1.3 \mu\text{m}$ and $\Lambda = 1.35 \mu\text{m}$. Fig. 6 shows its effective mode area A_{eff} and the nonlinear coefficient γ as a function of the wavelength. It is seen that the effective mode area A_{eff} increases and the nonlinear coefficient γ decreases with the increasing wavelength. At $2.9 \mu\text{m}$, A_{eff} of $7.83 \mu\text{m}^2$ and γ of $0.1257 \text{ m}^{-1}\text{W}^{-1}$ are obtained. Besides, our designed fluoride PCF has large normal dispersion, high nonlinearity and low confinement loss at the wavelength range from $2 \mu\text{m}$ to $3.2 \mu\text{m}$, indicating its broadband dispersion compensation potential.

3.2 Generation of Ultra-Short Pulses With PCF-Based Mode-Locked Fiber Laser

$3\text{-}\mu\text{m}$ mode-locked fiber laser usually operates at conventional soliton regime because of the large anomalous dispersion coefficient of fluoride fiber. Here we show the function of the PCF through achieving stretched pulse in a mode-locked fiber laser with dispersion management. The main virtue of stretched pulse is its dramatically compressed pulse duration compared with conventional soliton [26]. The simulation is implemented with nonlinear Schrodinger equation (NLSE) [27], which can be expressed as following:

$$\frac{\partial A}{\partial z} = -\frac{\alpha}{2}A - \frac{i\beta_2}{2}\frac{\partial^2 A}{\partial t^2} + \frac{\beta_3}{6}\frac{\partial^3 A}{\partial t^3} + i\gamma|A|^2A + \frac{g}{2}A + \frac{g}{2\Omega_g^2}\frac{\partial^2 A}{\partial t^2}, \quad (6)$$

where, A is the amplitude component of the optical pulses. α is the loss coefficient of the fiber. β_2 and β_3 denote the second and the third dispersion coefficient, respectively. γ refers to the cubic refractive nonlinearity of the medium. Ω_g is the bandwidth of the laser gain. The variable t and z indicate the time and the propagation distance, respectively. g is the net gain, which is nonzero only for the gain fiber. It describes the gain function of Er^{3+} -doped fiber and is expressed by $g = g_0 \exp(-E_p/E_s)$, where g_0 is the small-signal gain, E_p is the pulse energy, and E_s is the gain saturation energy which is pump power dependent [28].

This ring cavity design is illustrated in Fig. 7, which in order composed of a 8 m long Er^{3+} -doped fluoride fiber, a $9/1$ coupler, a saturable absorber (SA), and a 0.35 m ZBLAN PCF. The ZBLAN PCF is designed as the structure of $d_1 = 1 \mu\text{m}$, $d_2 = 1.3 \mu\text{m}$ and $\Lambda = 1.35 \mu\text{m}$, which the chromatic dispersion, three order dispersion, nonlinear coefficient and confinement loss of the designed PCF

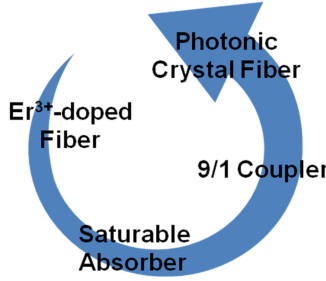


Fig. 7. Illustration of the fiber laser cavity elements used for the simulations.

at 2.9 μm are -351.3 ps/km/nm , $-4.4 \times 10^{-3} \text{ ps}^3/\text{m}$, $0.1257 \text{ m}^{-1}\text{W}^{-1}$, 0.05 dB/m , respectively. And the chromatic dispersion, three order dispersion, nonlinear coefficient, small gain coefficient, and gain bandwidth of the Er³⁺-doped gain fiber are set to be 15.38 ps/km/nm , $-0.28 \times 10^{-3} \text{ ps}^3/\text{m}$, $0.1258 \times 10^{-2} \text{ m}^{-1}\text{W}^{-1}$, 5 m^{-1} , and 7 THz , respectively. The net cavity dispersion is calculated to be -0.00035 ps^2 with PCF and -0.5488 ps^2 without PCF, respectively. The mode-locker in the simulation is assumed to be a simple two-level saturable absorber with the measured parameters of topological insulator in our previous work [29], which is expressed by [30]

$$\alpha(I) = \alpha_{ns} + \frac{\alpha_0}{1 + I/I_{sat}}, \quad (7)$$

where $\alpha(I)$ is the intensity-dependent absorption coefficient, and α_0 , α_{ns} and I_{sat} are the linear limit of saturable absorption, nonsaturable absorption, and saturation intensity, respectively. The values of saturable absorption, nonsaturable absorption, and saturation intensity are set to be 36.1%, 51.3%, and 2.12 MW/cm^2 , which are the same as the experimental measurement [29].

Slip-step Fourier method is employed to solve the Eq. (6). The simulation starts with an arbitrary weak signal, and ends with a self-consistent optical field. When we increase the value of Es, the pulse first becomes narrower with an increased peak power and finally breaks due to the pulse splitting effect [31]. Under the critical condition of pulse splitting, i.e., $Es = 101 \text{ pJ}$ without PCF and $Es = 89 \text{ pJ}$ with PCF, the pulse duration reaches its narrowest level. In this case, the output pulse evolutions are shown in Fig. 8. It is seen that the evolutions quickly converge from the weak initial signal to stable single pulse operation after the number of trip of ~ 20 , which indicates that the PCF has no influences on the stability of optical field. Fig. 8(b) shows the output pulse temporal profiles (curves in solid) and corresponding chirp distributions (curves in dashed) without and with PCF captured at the round trip number of 200. It is seen that the pulse duration is significantly compressed from 3.06 ps to 1.56 ps while the peak power increases from 5.71 W to 11.13 W with the help of PCF. Their chirps are nearly linear across the center part of the pulse, and the pulse chirp amount without PCF is far less than the pulse with PCF. The strong chirp distribution is also a typical feature of the stretched soliton regime. Fig. 8(c) shows the output optical spectra of the pulse with PCF and without PCF. Obvious Kelly sidebands on the spectrum without PCF are important sign of the conventional soliton regime, while the Gaussian-like spectrum profile with PCF is also a sign of typical stretched pulse regime. Their corresponding 3 dB bandwidths are 5.26 nm and 24.94 nm, respectively. To further compare the features of conventional soliton pulse and stretched pulse, we plot their pulse duration evolutions along the laser cavity, as shown in Fig. 8(d). It is observed that the conventional soliton and stretched pulse experience stretching and compressing once and twice, respectively. Compared with the conventional soliton which has a small stretching ratio of 1.1 (3.32 ps/3.12 ps), the stretched pulse has a large stretching ratio of 12.2(3.35 ps/0.275 ps). These features are consistent with the previous report about SP [32]. Fabricating the high quality ZBLAN microfiber is complex now, but with constant technological advances, we expect that the kind of fiber can be prepared with high yields and repeatability. Considering the practical applications in ultrafast fiber laser system, the insertion loss of ZBLAN PCF can be reduced by improving the fiber

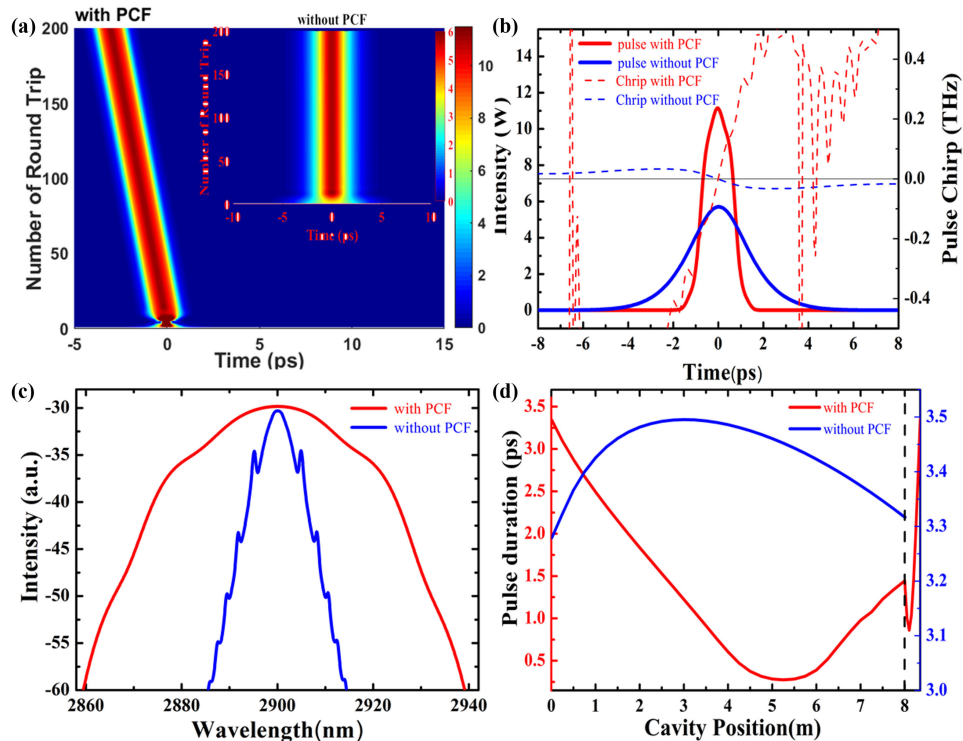


Fig. 8. (a) Process of soliton generation in the laser with PCF and without PCF (inset). (b) Output pulse profiles (curves in solid) and corresponding chirps distributions (curves in dashed) with and without PCF. (c) Output optical spectra of the pulse with and without PCF. (d) Comparison of pulse duration evolutions along the laser cavity with and without PCF.

preparation technique such as nanofabrication technique [33] or by adiabatic tapering the fiber waveguide [34].

4. Conclusion

In this paper, we design a kind of novel fluoride PCF, and numerically investigate its dispersion and confinement loss properties. By optimizing the geometric parameters using the full-vector finite-element method combined with perfectly matched layers boundary condition, the PCF with $d_1 = 1 \mu\text{m}$, $d_2 = 1.3 \mu\text{m}$, $\Lambda = 1.35 \mu\text{m}$ can give a large normal dispersion of -351.3 ps/km/nm and confinement loss of 0.05 dB/m at $2.9 \mu\text{m}$. When we use the PCF as a dispersion compensator in a Er^{3+} -doped mode-locked fiber laser, the output pulse can be compressed from 3.06 ps to 1.56 ps , indicating the potential of the designed PCF for dispersion management of mid-infrared ultra-short fiber lasers.

References

- [1] T. Hu, S. D. Jackson, and D. D. Hudson, "Ultrafast pulses from a mid-infrared fiber laser," *Opt. Lett.*, vol. 40, no. 18, pp. 4226–4228, 2015.
- [2] J. F. Li, D. D. Hudson, Y. Liu, and S. D. Jackson, "Efficient $2.87 \mu\text{m}$ fiber laser passively switched using a semiconductor saturable absorber mirror," *Opt. Lett.*, vol. 37, no. 18, pp. 3747–3749, 2012.
- [3] C. Wei, X. S. Zhu, R. A. Norwood, and N. Peyghambarian, "Passively continuous-wave mode-locked $\text{Er}(3+)$ -doped ZBLAN fiber laser at $2.8 \mu\text{m}$," *Opt. Lett.*, vol. 37, no. 18, pp. 3849–3851, 2012.
- [4] P. Tang *et al.*, "Watt-level passively mode-locked Er^{3+} -doped ZBLAN fiber laser at $2.8 \mu\text{m}$," *Opt. Lett.*, vol. 40, no. 21, pp. 4855–4858, 2015.

- [5] T. Hu, D. D. Hudson, and S. D. Jackson, "Stable, self-starting, passively mode-locked fiber ring laser of the 3 μm class," *Opt. Lett.*, vol. 39, no. 7, pp. 2133–2136, 2014.
- [6] G. Zhu *et al.*, "Graphene mode-locked fiber laser at 2.8 μm ," *IEEE Photon. Technol. Lett.*, vol. 28, no. 1, pp. 7–10, 2016.
- [7] J. Li *et al.*, "Black phosphorus: A two-dimension saturable absorption material for mid-infrared Q-switched and mode-locked fiber lasers," *Sci. Rep.*, vol. 6, no. 30361, 2016.
- [8] C. Zhu *et al.*, "A robust and tunable mid-infrared optical switch enabled by bulk Dirac fermions," *Nature Commun.*, vol. 8, no. 14111, 2017.
- [9] J. Liu and D. Y. Shen, "High-power and narrow-linewidth Er, Yb fiber laser locked by a volume Bragg grating-pair," *IEEE J. Quantum Electron.*, vol. 50, no. 2, pp. 88–91, 2014.
- [10] X. Y. Zhou, D. Yoshitomi, Y. Kobayashi, and K. Torizuka, "Generation of 28-fs pulses from a mode-locked ytterbium fiber oscillator," *Opt. Exp.*, vol. 16, no. 10, pp. 7055–7059, 2008.
- [11] K. C. Chu, H. Y. Jiang, and S. D. Yang, "High-energy femtosecond amplifier-similariton Er-doped fiber oscillator," *Opt. Lett.*, vol. 40, no. 22, pp. 5319–5322, 2015.
- [12] F. Haxsen, D. Wandt, U. Morgner, J. Neumann, and D. Kracht, "Pulse characteristics of a passively mode-locked thulium fiber laser with positive and negative cavity dispersion," *Opt. Exp.*, vol. 18, no. 18, pp. 18981–18988, 2010.
- [13] S. Kivisto, R. Herda, and O. G. Okhotnikov, "All-fiber supercontinuum source based on a mode-locked ytterbium laser with dispersion compensation by linearly chirped Bragg grating," *Opt. Exp.*, vol. 16, no. 1, pp. 265–270, 2008.
- [14] S. Duval, M. Olivier, M. Bernier, R. Vallee, and M. Piche, "Ultrashort pulses from an all-fiber ring laser incorporating a pair of chirped fiber Bragg grating," *Opt. Lett.*, vol. 39, no. 4, pp. 989–992, 2014.
- [15] R. Gumeyuk, I. Vartiainen, H. Tuovinen, and O. G. Okhotnikov, "Dissipative dispersion-managed soliton 2 μm thulium/holmium fiber laser," *Opt. Lett.*, vol. 36, no. 5, pp. 609–611, 2011.
- [16] L. Zhu *et al.*, "Generation of high fidelity 62-fs, 7-nJ pulses at 1035 nm for a net normal-dispersion Yb-fiber laser with anomalous dispersion higher-order-mode fiber," *Opt. Exp.*, vol. 21, no. 14, pp. 16255–16262, 2013.
- [17] J. Boguslawski, J. Sotor, G. Sobon, and K. M. Abramski, "80 fs passively mode-locked Er-doped fiber laser," *Laser Phys.*, vol. 25, no. 065104, 2015.
- [18] Y. X. Tang, A. Chong, and F. W. Wise, "Generation of 8 nJ pulses from a normal-dispersion thulium fiber laser," *Opt. Lett.*, vol. 40, no. 10, pp. 2361–2364, 2015.
- [19] Z. Zhang *et al.*, "All-fiber nonlinearity- and dispersion-managed dissipative soliton nanotube mode-locked laser," *Appl. Phys. Lett.*, vol. 107, no. 241107, 2015.
- [20] F. Stutzki *et al.*, "Tm-based fiber-laser system with more than 200 MW peak power," *Opt. Lett.*, vol. 40, no. 1, pp. 9–12, 2015.
- [21] Z. X. Zhang, C. Senel, R. Hamid, and F. O. Ilday, "Sub-50 fs Yb-doped laser with anomalous-dispersion photonic crystal fiber," *Opt. Lett.*, vol. 38, no. 6, pp. 956–958, 2013.
- [22] X. Jiang, N. Y. Joly, M. A. Finger, and G. K. L. Wong., "Deep ultraviolet to mid infrared supercontinuum generated in solid-core ZBLAN photonic crystal fibre," *Nature Photon.*, vol. 9, pp. 133–139, 2015.
- [23] Q. L. Yang, L. L. Miao, G. B. Jiang, and C. J. Zhao, "Modeling the broadband mid-infrared dispersion compensator based on ZBLAN microfiber," *IEEE Photon. Technol. Lett.*, vol. 28, no. 7, pp. 728–731, 2016.
- [24] D. C. Tee, N. Tamchek, and C. H. Raymond Ooi, "Numerical modeling of the fundamental characteristics of ZBLAN photonic crystal fiber for communication in 2–3 μm midinfrared region," *IEEE Photon. J.*, vol. 8, no. 2, no. 2536940, 2016.
- [25] H. Saghaei, M. Ebnnali-Heidari, and M. K. Moravvej-Farshi, "Midinfrared supercontinuum generation via As_2Se_3 chalcogenide photonic crystal fibers," *Appl Opt.*, vol. 54, no. 8, pp. 2072–2079, 2015.
- [26] M. Olivier, V. Roy, M. Piché, and F. Babin, "Pulse collisions in the stretched-pulse fiber laser," *Opt. Lett.*, vol. 29, no. 13, pp. 1461–1463, 2004.
- [27] D. Y. C. Ma, X. Tian, B. Gao, and G. Wu, "Dynamic evolution of the dissipative soliton in passively mode-locked fiber laser based on black phosphorus as a new saturable absorber," *Opt. Commun.*, vol. 406, pp. 177–182, 2018.
- [28] H. Chen *et al.*, "Buildup dynamics of dissipative soliton in an ultrafast fiber laser with net-normal dispersion," *Opt. Exp.*, vol. 26, no. 3, pp. 2972–2982, 2018.
- [29] J. Li *et al.*, "3- μm mid-infrared pulse generation using topological insulator as the saturable absorber," *Opt. Lett.*, vol. 40, no. 15, pp. 3659–3662, 2015.
- [30] Z. Kang *et al.*, "Passively Q-switched erbium doped fiber laser using a gold nanostars based saturable absorber," *Photon. Res.*, vol. 6, no. 6, pp. 549–553, 2018.
- [31] Y. Z. Wang, J. F. Li, and H. Y. Luo, "Coexistence of dissipative soliton and stretched pulse in dual-wavelength mode-locked Tm-doped fiber laser with strong third-order dispersion," *Opt. Exp.*, vol. 26, no. 14, pp. 18190–182201, 2018.
- [32] B. G. Bale, S. Boscolo, and S. K. Turitsyn, "Dissipative dispersion-managed solitons in mode-locked lasers," *Opt. Lett.*, vol. 34, no. 21, pp. 3286–3288, 2012.
- [33] M. Yaman, T. Khudiyev, E. Ozgur, M. Kanik, O. Aktas, and E. O. Ozgur, "Arrays of indefinitely long uniform nanowires and nanotubes," *Nature Mater.*, vol. 10, no. 7, pp. 494–501, 2011.
- [34] M. Liu *et al.*, "Demonstration of multiwavelength erbium-doped fiber laser based on a microfiber knot resonator," *IEEE Photon. Technol. Lett.*, vol. 26, no. 14, pp. 1387–1390, 2014.